Recent results from the Berkeley 0.3-NA EUV microfield exposure tool

Patrick P. Naulleau,[1] Christopher N. Anderson,[2] Kim Dean,[3] Paul Denham,[1]
Kenneth A. Goldberg,[1] Brian Hoef,[1] Bruno La Fontaine,[4] and Tom Wallow[4]

[1]Center for X-Ray Optics, Lawrence Berkeley National Laboratory, Berkeley, CA 94720
[2]Applied Science & Technology Dept., University of California, Berkeley, CA 94720
[3]SEMATECH, Austin, TX 78741
[4]Advanced Micro Devices, Sunnyvale, CA 94088

ABSTRACT

Operating as a SEMATECH resist test center, the Berkeley 0.3-NA EUV microfield exposure tool continues to play a crucial role in the advancement of EUV resists and masks. Here we present recent resist-characterization results from the tool as well as tool-characterization data. In particular we present lithographic-based aberration measurements demonstrating the long-term stability of the tool. We also describe a recent upgrade to the tool which involved redesign of the programmable coherence illuminator to provide improved field uniformity as well as a programmable field size.

Keywords: extreme ultraviolet, lithography, photoresist, aberrations, illuminator

1. INTRODUCTION

With the entry node for extreme ultraviolet (EUV) lithography being pushed towards smaller nodes, resist issues become an ever more important component of the overall EUV technology development task. In 2005, the ability to simultaneously achieve the required resolution, sensitivity, and LER was determined to be the highest risk potential roadblock to the commercialization of EUV lithography [1]. In 2006 we saw significant improvements in EUV resists resulting in resists dropping to number two on the list of potential roadblocks [2]. Despite these improvements, it is evident that resists remain an area of significant concern for EUV.

Microfield exposure tools [3-5] play a particularly important role in the area of resist development. This is due to the fact that the relative simplicity of such tools in general enables them provide higher resolution capabilities than full production scale alpha tools. For example, preproduction/alpha tools just now being developed/delivered [6,7] have numerical apertures (NA) of 0.25 as compared to the 0.3-NA available from the latest EUV microfield exposure tools.

One of the most productive and highest performing EUV microfield exposure tools available has been the Berkeley MET tool [3,8,9] operating as a SEMATECH resist test center since early 2004. The Berkeley exposure tool utilizes SEMATECH's 5×-reduction, 0.3-NA Micro-Exposure Tool (MET) optic [10, 11]. The MET optic has a well-corrected field of view of 1×3 mm at the reticle plane (200×600 μm at the wafer plane). The CAD model shown in Figure 1 depicts the major

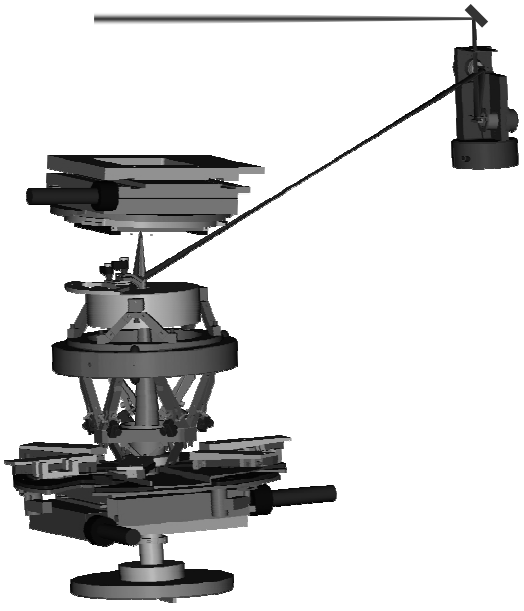

Fig. 1. CAD model of the Berkeley MET exposure tool.

Emerging Lithographic Technologies XI, edited by Michael J. Lercel,
Proc. of SPIE Vol. 6517, 65170V, (2007) · 0277-786X/07/$18
doi: 10.1117/12.713440

components of the exposure station as well as the EUV beam path (the system is described in detail in Ref. 3). With a NA of 0.3, the MET optic has a Rayleigh resolution (k_1 factor = 0.61) of 27 nm.

Although the Berkeley MET tool utilizes the same projection optics design as used by commercial MET tools [4], the Berkeley MET tool has some unique characteristics owing to the fact that it uses the Advanced Light Source synchrotron facility as its light source as opposed to a conventional EUV discharge source. The use of coherent synchrotron radiation [12] in setting up the tool allowed *in-situ* actinic wavefront metrology to be performed ensuring the optimal alignment of the tool. Even more importantly, the coherent source enabled the implementation of a programmable coherence (pupil fill) illuminator [13]. This unique illuminator supports the generation of arbitrary pupil fills in a lossless manner. For example, extreme dipole or off-axis illuminations are easily implemented enabling the k_1 factor to be pushed all the way to its theoretical limit of 0.25. At such an aggressive k_1 factor, the resolution limit of the tool becomes 11 nm. Given that EUV resolution is presently resist limited [8], we have not yet been able to demonstrate printing at such small k_1 factors. In practice, resist limits have restricted us to k_1 factors of approximately 0.5 and larger.

2. RECENT RESIST TESTING RESULTS

As stated above, significant improvements have been made in resists over the past year. Figure 2 shows results of two experimental resists (kindly supplied by Rohm and Haas and TOK) exposed using the Berkeley MET tool, demonstrating resolution down to 28 nm half pitch. For both of these materials, the failure mechanism appears to be pattern collapse either at, or slightly below 28 nm half-pitch, suggesting that the intrinsic resolution limit of the resist would support even better resolution. Unfortunately, we have not yet had the opportunity to perform the MTF or corner-rounding tests [14] on these resists and thus cannot directly comment on the estimated intrinsic resolution limits.

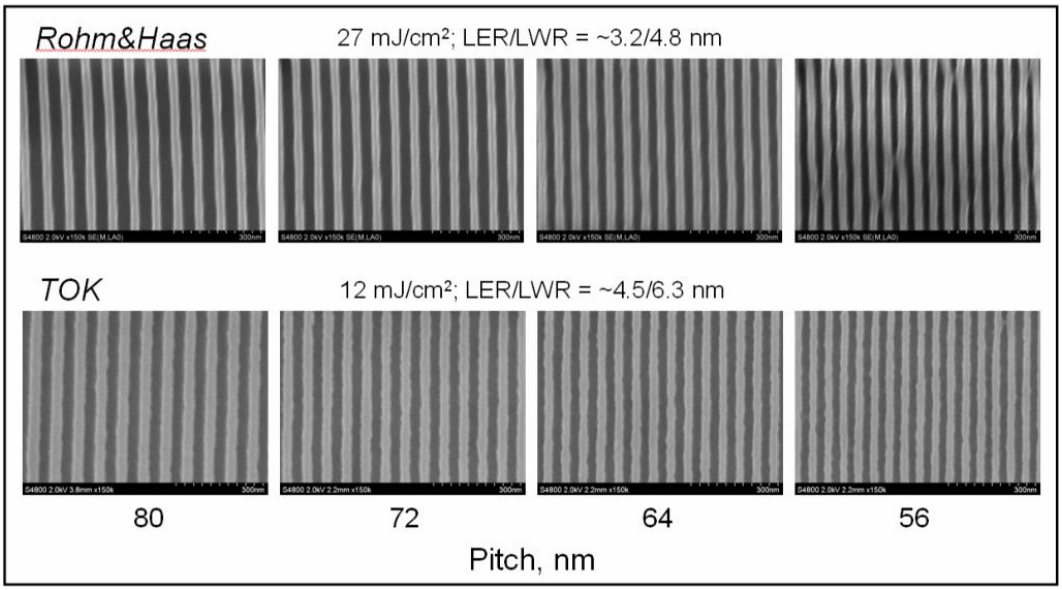

Fig. 2. Through-pitch resolution of newer generation resists. Film thickness for Rohm and Haas resist is 50 nm; film thickness for TOK resist is 80 nm. Both resists were exposed using Y-monopole illumination.

Although resist resolution supporting the 32-nm node requirements has now been demonstrated, LER remains a significant issue. The well-known trade-offs in resist design between resolution, speed, and LER strongly motivate the use of alternative techniques for LER reduction. An example of such a technique is the use of surface conditioner rinses. Application of such rinses has been demonstrated to smooth LWR for a variety of 193 nm and 248 nm resists [15,16]. Figure 3 shows that significant LER reduction can also be accomplished at EUV. Note that approximately 1 nm (3σ) LER and 1.5 nm (3σ) LWR reduction is observed for 40 nm 1:1 line/space features in this example.

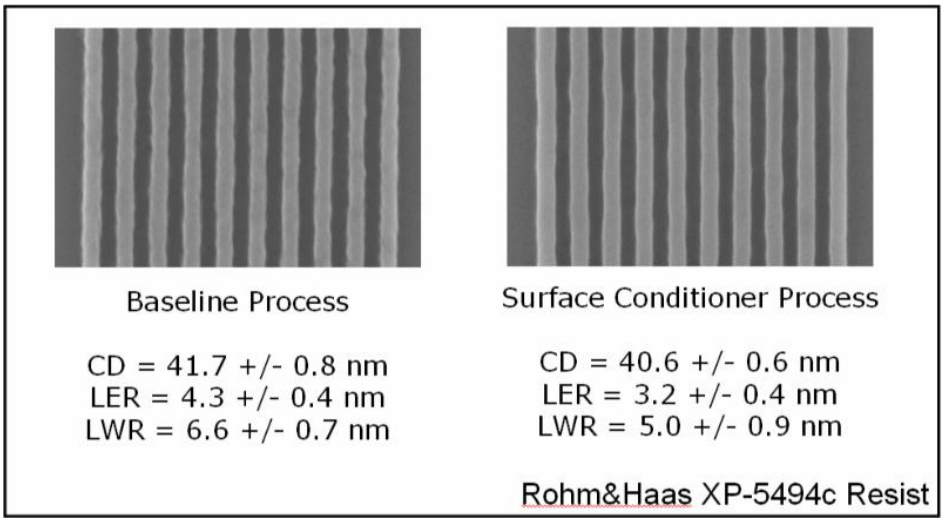

Fig. 3. Roughness reduction in an EUV resist using a surface conditioner rinse.

Comparison of the original and smoothed power spectral densities (Fig. 4) shows that smoothing occurs predominantly in mid-spatial frequencies, but that noticeable smoothing is also seen at low spatial frequencies. The smoothing at low spatial frequencies is a departure from previous studies at 193 nm [17] and requires additional explanation.

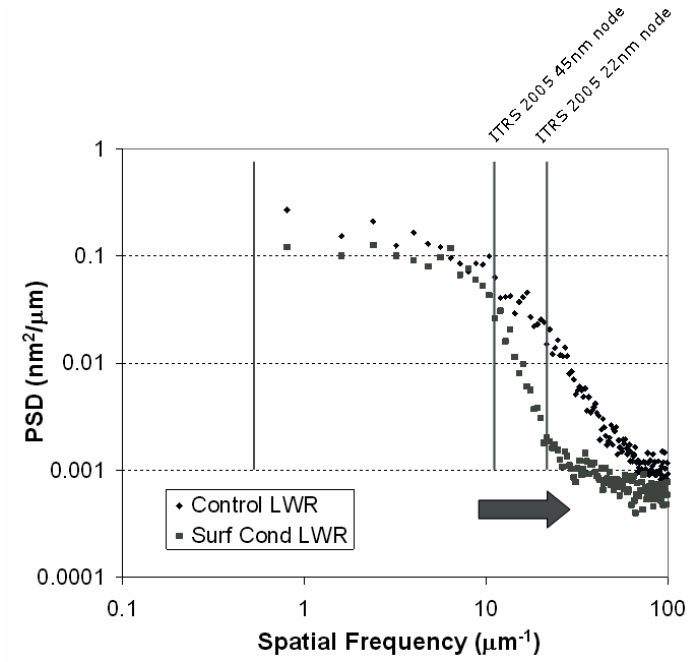

Fig. 4. LWR power spectral densities for smoothed and unsmoothed EUV resist features.

3. ALINGNMENT STABILITY IN THE SEMATECH BERKELEY MET TOOL

Last year we reported on the lithographic characterization of low order aberrations in the SEMATECH Berkeley MET tool [18]. The results showed evidence of alignment change between at-wavelength interferometry and lithography. It was not evident, however, if this change was discrete, for example, as a result of handling of the optic during transition from interferometry to lithography configurations or due to a more gradual alignment drift that could continue to impact the tool. To address this question we have repeated a portion of the lithographic measurements 1 year later. In particular, we have re-characterized the astigmatism over the central portion of the field. We have chosen astigmatism owing to the fact that of the two aberrations observed to have changed since the interferometry (astigmatism and spherical error, no change was observed in coma) [18], the astigmatism measurement is believed to be the more precise and accurate lithographic measurement.

To characterize the astigmatism (magnitude and direction) one must obtain the relative longitudinal focal positions of four orthogonal feature orientations, for example, 0°, 90°, -45°, and 45°. As shown in Figure 5, the close proximity 0° and 45°-oriented elbow patterns in the SEMATECH MET dark-field mask are suitable for this task. To provide through-focus feature-size data, we print a focus-exposure matrix (FEM) with focus steps of 30 nm. At a dose safely away from the iso-focal value, we measure the printed linewidth, or critical dimension (CD), and line-edge-roughness (LER) from each arm of 0° and 45°-oriented 50 nm elbow patterns through focus for each of the central field cites. For each feature orientation, the through-focus CD and LER data are fit to second order polynomials whose minima give the measured longitudinal plane of best focus. The relative shift in best-focus planes for 0°/90° and -45°/45° features, multiplied by the modeled .5 nm rms astigmatism per 55 nm relative orthogonal-feature focal shift [20] gives the measured rms astigmatism at 0° and 45°, respectively.

The above procedure has been used to measure 0° and 45° astigmatism at the three central field cites of the SEMATECH Berkeley MET tool. Figure 6 shows the through-focus CD and LER data for -45° and 45° features at a field site that is representative of typical data throughout the collection window. As depicted here, we generally find good agreement between measured focus-offset as determined by CD and LER data. Figure 7 shows the measured astigmatism across the three measured central field sites. Both individual astigmatism components as well as the total astigmatism magnitudes are shown. For comparison, we also show the astigmatism results reported one year ago using the same lithographic characterization method [18].

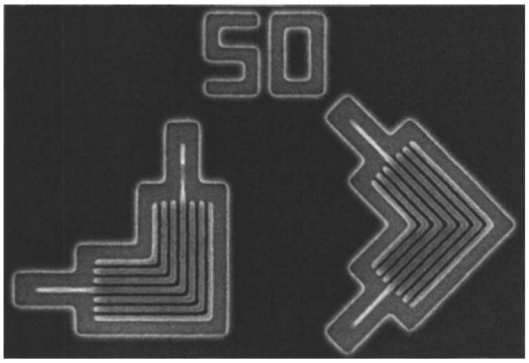

Fig. 5. Scanning electron microscope (SEM) image of the printed elbow features used to extract the astigmatism data. The 0° and 45°-oriented elbow patterns are placed in close proximity on the mask to ensure that dose and focus can be assumed constant over the features of interest.

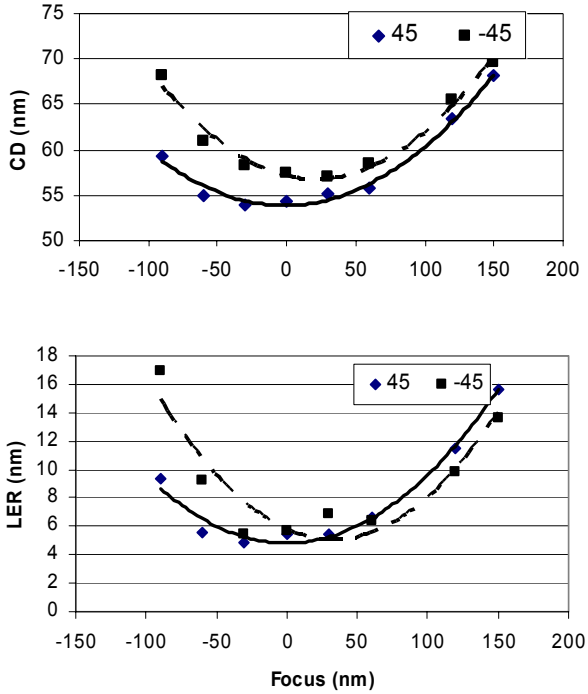

Fig. 6. Through-focus CD and LER data with quadratic fits for one field point representative of the 3 x 1 grid of measured central field points. The –45° and 45° feature are data is shown, corresponding to 45° astigmatism.

0° astigmatism	7 / 2006		5 / 2005		Difference	
	-0.344		-0.434		-0.091	
	-0.351		-0.427		-0.076	
	-0.341		-0.511		-0.170	
45° astigmatism						
	-0.242		-0.237		0.005	
	-0.152		-0.079		0.073	
	-0.022		-0.089		-0.067	
Total astigmatism magnitude						
	0.420		0.494		-0.074	
	0.383		0.433		-0.050	
	0.341		0.518		-0.177	

Fig. 7. Lithographically measured astigmatism at three central points in the field. Reported results are rms magnitudes in nm. The locations in the table correspond to the physical locations of the measured site in the field. For comparison, we include last year's results [18] and the difference between the new and old values

Comparing the new results with those obtained a year ago, we see that all new measured values are within the reported 0.1 nm measurement uncertainty with the exception of the bottom field site at 0°. For the bottom field site, which had the largest reported 0° rms astigmatism of all sites one year ago, we observe a 0.17-nm decrease in 0° rms astigmatism, roughly twice the magnitude of the measurement uncertainty reported last year. Within the uncertainty of our measurement, there is no evidence of significant alignment drift in the Berkeley MET tool.

Over the past year we have also tracked focus stability of the tool. Figure 8 shows tracking data obtained from a periodically performed baseline process. The day-to-day rms stability is found to be 90 nm. A gradual drift of 200-nm over the year is observed.

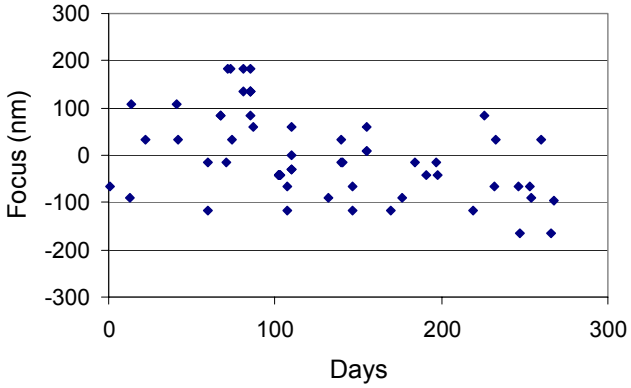

Fig. 8. Focus tracking data obtained from a periodically performed baseline process on the SEMATECH Berkeley MET tool. Day-to-day rms stability is 90 nm.

4. ILLUMINATOR UPGRADE

Although designed to provide a programmable pupil fill [13], the highly coherent undulator beamline [12] the SEMATECH Berkeley MET tool is installed on significantly complicates the achievement of uniform illumination due to coherence artifacts arising prior to the pupil-fill scanner mechanism. To address this issue a new field integrating optical subsystem has been added to the beamline prior to the pupil-fill control group. As described below, this new optical subsystem enables both improved uniformity and an adjustable field size.

With the goal of increasing tool utility and reproducibility on a day-to-day basis, we've implemented a scanning fly's eye illuminator subsystem enabling robust, uniform illumination over the entire 3-mm × 1-mm object-side field of the SEMATECH Berkeley MET tool. As depicted in Figure 9, the non-ideal illumination footprint arriving from upstream beamline optics strikes at a pair of diamond-turned cylindrical lenslet arrays that map small neighboring sections of the incoming footprint to an overlap region on the surfaces of the Fourier-synthesis scanning mirrors. In this configuration, each lenslet pair (one in x and one in y) creates a spherical-like wavefront emanating towards the Fourier-synthesis mirrors with an amplitude given by the incoming illumination intensity at the local lenslet site. The far-field spatial overlap of all the spherical-like wavefronts gives rise to a highly uniform fill in the overlap region on the Fourier-synthesis scanning mirrors. To eliminate unwanted interference between spherical-like wavefronts emerging from different lenslet sites, we longitudinally offset each lenslet in the fly's eye array by the illumination coherence length of approximately 500-nm.

We've enabled moderate control of the illuminated field size by designing the fly's eye uniformity stage to fill a 1-mm x 1-mm subset of the 1-mm x 3-mm usable field. The fly's eye lenses are mounted to programmable scanners similar to those used to control coherence [13] enabling customizable field offset and fill control. The rough diamond-turned surfaces of the fly's eye lenslets are rendered suitable for multilayer deposition with an in house smoothing technique. [21]. We maximize the illuminator efficiency by using the up-stream Kirkpatrick-Baez mirrors as field lenses, mapping the footprints of all the spherical-like wavefronts emerging from different lenslets to the same 1-mm × 1-mm location in the reticle.

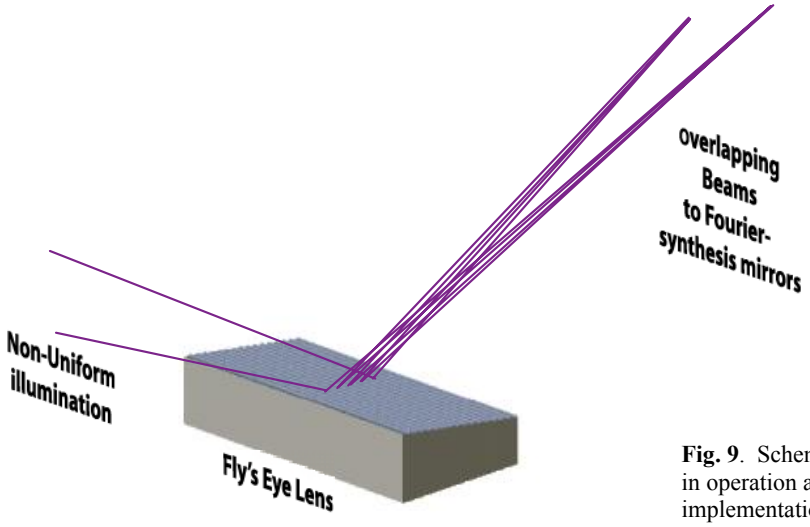

Fig. 9. Schematic of conventional fly's eye lens in operation and a 1D ray trace schematic of our implementation scheme at the SEMATECH Berkeley MET tool. Non-uniform light from upstream optics strikes one of two fly's eye lenses producing homogenized illumination downstream.

5. SUMMARY

The SEMATECH Berkeley tool continues to play a crucial role in the advancement of EUV. The unique programmable coherence properties of this tool enable it to achieve higher resolution than other 0.3-NA EUV tools. Over the past year the tool has been used to demonstrate resist resolutions of 28 half pitch and alternative approaches to LER reduction. Moreover, as presented elsewhere [19] the SEMATECH Berkeley tool has demonstrated as-coded 22.5-nm semi-isolated printing in a chemically amplified resist with a sensitivity of 19 mJ/cm^2.

The long term aberration stability of the tool has also been verified through lithographic measurement of astigmatism. Results show no long term aberration drift. Moreover, the illuminator has been upgraded to provide improved field uniformity as well as an adjustable field size through the use of an additional scanning field integrating optical system.

The authors are greatly indebted to Gideon Jones, and Jerrin Chiu of the Center for X-Ray Optics at Lawrence Berkeley National Laboratory for expert support with the exposure tool. We are also owe many thanks to the precision engineering team including Seno Rekawa, Kevin Bradley, Rene Delano, Gideon Jones, Drew Kemp, Ron Oort, and Ron Tackaberry for implementation of the new illuminator. Moreover we thank Farhad Salmassi and Eric Gullikson for multilayer coating support for the new illuminator optics. This work was funded by SEMATECH and performed at Lawrence Berkeley National Laboratory using the SEMATECH MET exposure facility at the Advanced Light Source. Lawrence Berkeley National Laboratory is operated under the auspices of the Director, Office of Science, Office of Basic Energy Science, of the US Department of Energy.

REFERENCES

1. 4th International EUVL Symposium Steering Committee, San Diego, CA, November 7-9, 2005, proceedings available from SEMATECH, Austin, TX.
2. 2006 International Symposium on Extreme Ultraviolet Lithography Steering Committee, Barcelona, Spain, October 15-18, 2006, proceedings available from SEMATECH, Austin, TX.
3. P. Naulleau, *et al.*, "Status of EUV micro-exposure capabilities at the ALS using the 0.3-NA MET optic," Proc. SPIE **5374**, 881-891 (2004).
4. A. Brunton, *et al*., "High-resolution EUV imaging tools for resist exposure and aerial image monitoring," Proc. SPIE **5751**, 78-89 (2005).
5. H. Oizumi, Y. Tanaka, I. Nishiyama, H. Kondo, K. Murakami, "Lithographic performance of high-numerical-aperture (NA=0.3) EUV small-field exposure tool (HINA)," Proc. SPIE **5751**, 102-109 (2005).
6. H. Meiling, *et al*., "First performance results of the ASML alpha demo tool," Proc. SPIE **6151**, 615108 (2006).
7. M. Miura, K. Murakami, K. Suzuki, Y. Kohama, Y. Ohkubo, T. Asami, "Nikon EUVL development progress summary," Proc. SPIE **6151**, 615105 (2006).
8. P. Naulleau, K. Goldberg, E. Anderson, K. Dean, P. Denham, J. Cain, B. Hoef, K. Jackson, "Characterization of the synchrotron-based 0.3 numerical aperture extreme ultraviolet microexposure tool at the Advanced Light Source," J. Vac. Sci. & Technol. B **23**, 2840-2843 (2005).
9. J. Cain, P. Naulleau, C. Spanos, "Resist-based measurement of the contrast transfer function in a 0.3-numerical aperture extreme ultraviolet microfield optic," J. Vac. Sci. & Technol. B **24**, 326-330 (2006).
10. J. Taylor, D. Sweeney, R. Hudyma, L. Hale, T. Decker, G. Kubiak, W. Sweatt, N. Wester, "EUV Microexposure Tool (MET) for near-term development using a high NA projection system," 2nd International EUVL Workshop October 19-20, 2000, proceedings available from SEMATECH, Austin, TX.
11. R. Hudyma, J. Taylor, D. Sweeney, L. Hale, W. Sweatt, N. Wester, "E-D characteristics and aberration sensitivity of the Microexposure Tool (MET)," 2nd International EUVL Workshop October 19-20, 2000, proceedings available from SEMATECH, Austin, TX.
12. D. Attwood, G. Sommargren, R. Beguiristain, K. Nguyen, J. Bokor, N. Ceglio, K. Jackson, M. Koike, and J. Underwood, "Undulator radiation for at-wavelength interferometry of optics for extreme-ultraviolet lithography," Appl. Opt. **32**, 7022-7031 (1993).
13. P. Naulleau, K. Goldberg, P. Batson, J. Bokor, P. Denham, and S. Rekawa, "A Fourier-synthesis custom-coherence illuminator for EUV microfield lithography," Appl. Opt. **42**, 820-826 (2003).
14. P. Naulleau, C. Anderson, B. La Fontaine, R. Kim, T. Wallow, "Lithographic metrics for the determination of intrinsic resolution limits in EUV resists," *these proceedings*.

15. P. Zhang, M. B. Rao, M. Jaramillo Jr., B. Horvath, B. Ross, T. Paxton, T. Davis, P. Cook, D. Witko, "Pattern Collapse and Line Width Roughness Reduction by Surface Conditioner Solutions for 248 nm Lithography," Proc. SPIE **5753**, 252, (2005).
16. P. Wong, W. Gehoel, S. Sinkwitz, P. Zhang, M. Jaramillo Jr., M. B. Rao, B. Horvath, B. Ross, S. Cassel, "Linewidth Roughness Reduction at the 55nm Node Through Combination of Classical Process Optimization and Application of Surface Conditioner Solutions," Proc. SPIE **6153**, 61533V, (2006).
17. P. Zhang, M. Jaramillo, S. Cassel, T. Wallow, A. Acheta, A. R. Pawloski, S. Bell, R.-H. Kim, "Post-Etch LER Performance of Novel Surface Conditioner Solutions," Proc. SPIE **6153**, 61533Y, (2006).
18. P. Naulleau, J. Cain, K. Dean, and K. Goldberg, "Lithographic Characterization of Low-Order Aberrations in a 0.3-NA EUV Microfield Exposure Tool," Proc. SPIE **6151**, 6151104 (2006).
19. P. Naulleau, C. Anderson, R. Kim, B. La Fontaine, T. Wallow, "Investigation of lithographic metrics for the characterization of intrinsic resolution limits in EUV resists," 2006 International Symposium on Extreme Ultraviolet Lithography, Barcelona, Spain, October 15-18, 2006, proceedings available from SEMATECH, Austin, TX.
20. Aerial image modeling was performed using the PROLITH modeling package from KLA-Tencor, San Jose, CA 95134.
21. F. Salmassi, P. Naulleau, E. Gullikson, "Spin-on-glass coatings for the generation of super-polished substrates for use in the extreme ultraviolet regime," Appl. Opt. **45**, 2404-2408 (2005).